Role of Twinning on Dynamic Recrystallization and Microstructure During Moderate to High Strain Rate Hot Deformation of a Ti-Modified Austenitic Stainless Steel

SUMANTRA MANDAL, A.K. BHADURI, and V. SUBRAMANYA SARMA

This article discusses the role of twinning on dynamic recrystallization (DRX) and microstructural evolution during moderate to high strain rate (0.1 to 100 s^{-1}) hot deformation (1173 to 1373 K (900 to 1100 °C) range) in a Ti-modified austenitic stainless steel (alloy D9). The extent of DRX increased with increasing strain rate and temperature in the range of hot working parameters employed in the present study. The acceleration of DRX with strain rate is attributed to increased rate of dislocation accumulation during high strain rate deformation as well as adiabatic temperature rise. The DRX grains were found to be twinned and a linear relationship was observed between the area fraction of DRX grains and the fraction of $\Sigma 3$ boundaries. Analysis of misorientations revealed that the majority of these $\Sigma 3$ boundaries are newly formed coherent twin boundaries during DRX. Interaction of pre-existing $\Sigma 3$ boundaries that may regenerate new $\Sigma 3$ boundaries did not seem to occur frequently during DRX. The majority of the twin boundaries are found within the DRX grains, signifying that these annealing twins are mainly formed by "growth accidents" during the expansion of the DRX grains. It is suggested that annealing twins play an important role during nucleation and subsequent expansion of the DRX process in alloy D9.

I. INTRODUCTION

THE szoundness of components and their in-service performance largely depend on the thermomechanical processing adopted for their fabrication. During thermomechanical processing, the material undergoes shape and microstructural changes depending on the processing history. Therefore, attention should be directed toward the optimization of the process parameters such as temperature, strain, and strain rate to achieve a defect-free component with the desired microstructure. In low stacking fault energy (SFE) fcc alloys such as austenitic stainless steels, dynamic recrystallization (DRX) occurs readily during hot working. This is because dynamic recovery is sluggish (as climb and cross-slip are inhibited) and the driving force for recrystallization is maintained.[1] The phenomenon of DRX is technologically important, because it softens metals during hot deformation and reduces the hot working loads.[2] Further, it can lead to significant refinement of the microstructure, which improves the mechanical properties and formability of the materials.[3,4] The microstructure control through DRX requires detailed knowledge of microstructural evolution as a function of process parameters (*i.e.*, strain, strain rate, and temperature). Special emphasis needs to be given on understanding the nucleation mechanisms during DRX.

The influence of strain rate on DRX as a function of temperature and strain in the low strain rate domain (10^{-5} to 1 s^{-1}) was studied in detail in different materials.[5–7] It was observed that the fraction of recrystallized grains increased with the decrease in strain rate in the ranges 10^{-3} to 1 s^{-1} in Superalloy 718.[5] While studying the DRX behavior in Mg alloy, Beer and Barnett[6] also observed that the size of the DRX grains and the percentage of DRX increased with a decrease in strain rate in the range of 0.01 to 1 s^{-1}. Miura *et al.*[7] observed that the nucleation of DRX grains became more significant (*i.e.*, DRX becomes easier) in the Cu alloy bicrystal with the decrease in strain rate in the range of 4×10^{-5} to $4 \times 10^{-3} \text{ s}^{-1}$. The acceleration of DRX at lower strain rates is attributed to the decrease in the critical dislocation density and consequent lowering of the critical strain required for the occurrence of DRX. In addition, the lower strain rate provided longer times for nucleation and growth of DRX grains. Although the influence of strain rate on DRX in the lower strain rate domain seems to be well established, the influence of strain rate on DRX at higher strain rates ($\geq 1 \text{ s}^{-1}$) is not clear. This could be attributed largely to the fact that reports on the influence of strain rate ($>1 \text{ s}^{-1}$) on microstructural evolution and DRX during hot deformation are not well documented in open literature.

The understanding of microstructural evolution during moderate to high strain rate hot deformation is technologically important, since development of high strain rate thermomechanical processing will contribute

SUMANTRA MANDAL, Scientific Officer – E, and A.K. BHADURI, Associate Director, are with the Materials Technology Division, Indira Gandhi Centre for Atomic Research, Kalpakkam 603102, India. Contact e-mail: sumantra@igcar.gov.in V. SUBRAMANYA SARMA, Associate Professor, is with the Department of Metallurgical and Materials Engineering, Indian Institute of Technology Madras, Chennai 600036, India.

to an increase in productivity and reduce manufacturing costs. It was speculated by Pinheiro et al.[2] that DRX would become insignificant above a critical strain rate at a particular temperature. From the experimental data obtained at 100 s^{-1}, it was speculated that DRX would be insignificant above 200 s^{-1} at 1223 K (950 °C) in interstitial-free steel.[2] However, this has not been validated experimentally. On the other hand, the DRX was found to be enhanced during very high strain rate (~10^4 s^{-1}) hot deformation of Cu.[8] The acceleration of DRX in this condition was caused by adiabatic temperature rise.

Extensive research was carried out in the past to understand the mechanism of DRX.[9–16] It is established that nucleation of new DRX grains takes place predominantly on the parent grain boundaries by the "bulging mechanism."[12–14] This mechanism is able to describe how the first recrystallized grains and, correspondingly, the first layer of new recrystallized grains form. However, this mechanism could not account for the expansion of the necklace structure throughout the deformed matrix. This is because, in the course of DRX, when pre-existing grain boundaries are entirely covered by new grains (i.e., site saturation), bulging would have to proceed from the small recrystallized grains, and this requires a very high boundary curvature. This makes further nucleation by bulging unlikely, because the very high driving force necessary to offset the high surface tension of the bulge is not available in hot-deformed microstructures.[15] The crucial step for nucleation of DRX in a subgrain structure is the generation of a mobile grain boundary. For small-angle boundaries, the mobility increases with increasing misorientation, but a rotation of 10 to 15 deg is commonly assumed to be necessary for nucleation to occur.[16,7] Subgrain misorientation measurements in a dynamically recrystallized austenitic steel "alloy 800H"[18] and Superalloy 718[5] revealed that there was essentially no increase in the frequencies of misorientation angles in excess of 10 deg with increasing strain. Thus, a continuous subgrain rotation near the high-angle boundaries cannot be confirmed to be an active nucleation mechanism of DRX. In contrast to this, a high fraction of $\Sigma 3$ boundaries was observed in DRX microstructures of different low SFE materials.[5,18,19] It is believed that these $\Sigma 3$ boundaries play a crucial role to promote the expansion of the recrystallization front during DRX. However, the origin of these $\Sigma 3$ boundaries and their role is not well understood/established.

The objective of this study is to understand and evaluate the influence of strain rate on microstructure and DRX in a Ti-modified austenitic stainless steel (commonly known as alloy D9 used for in-core applications such as fuel cladding tube and hexagonal subassembly wrapper in Indian prototype fast breeder reactor) in a range of temperatures and strains during moderate to high strain rate (in the range of 0.1 to 100 s^{-1}, typically encountered during industrial scale thermomechanical processing) hot deformation. The evolution of twin boundaries and their role on DRX during hot deformation in alloy D9 were studied in detail.

II. EXPERIMENTAL

The chemical composition (weight percent) of alloy D9 is given in Table I. Hot compression tests were conducted on solution-annealed (SA) alloy D9 specimens of 15-mm height and 10-mm diameter in a Gleeble thermomechanical simulator (Dynamic Systems Inc., Poestenkill, NY). Concentric grooves of 0.5-mm depth were made on the top and bottom faces of these cylindrical specimens to facilitate the retention of lubricant during testing. A 1 mm–45 deg chamfer was provided along the edges of the top and bottom faces to avoid foldover of the material in the initial stages of compression. The uniaxial compression tests were performed in the temperature ranges of 1173 to 1373 K (900 to 1100 °C) (in steps of 100 K) at strain rates of 0.1, 1, 10, and 100 s^{-1}. Various degrees of deformation (true strains of 0.2, 0.4, 0.6, and 0.8) were imparted at each temperature and strain rate to study the influence of strain on microstructural evolution in alloy D9. The specimens were heated at a rate of 5 K s^{-1}. Before imparting the deformation, every specimen was held for 3 minutes at the test temperature to achieve homogeneous temperature distribution throughout the specimen. To minimize the friction, graphite foil (5/10 mil) in combination with high-temperature lubricants (MoS_2) was used. It should be noted here that no significant barrelling of the specimen was observed following uniaxial compression deformation. The hot-deformed specimens were water quenched with a spray nozzle as soon as the specified amounts of strains were imparted (within ~1 to 2 seconds) in order to freeze the hot-deformed microstructure. It may be noted that this is the best possible experimental condition that can be realized to preserve the hot-deformed microstructure.

The schematic representation of the specimen before and after the uniaxial compression testing is shown in Figures 1(a) and (b), respectively. The hot-deformed samples were cut along the longitudinal direction (as shown by the dotted line in Figure 1(b)) using a Secotom-10 table top precision cut-off machine. One half of the sample (shown in Figure 1(c)) was taken to prepare specimens for electron backscattered diffraction (EBSD) investigation. The microstructures were examined in the maximum deformation zone of the specimens (marked "X" in Figure 1(c)). EBSD scans were performed on all

Table I.   Chemical Composition (Weight Percent) of 15Cr-15Ni-2.2Mo-Ti Modified Austenitic Stainless Steel (Alloy D9)

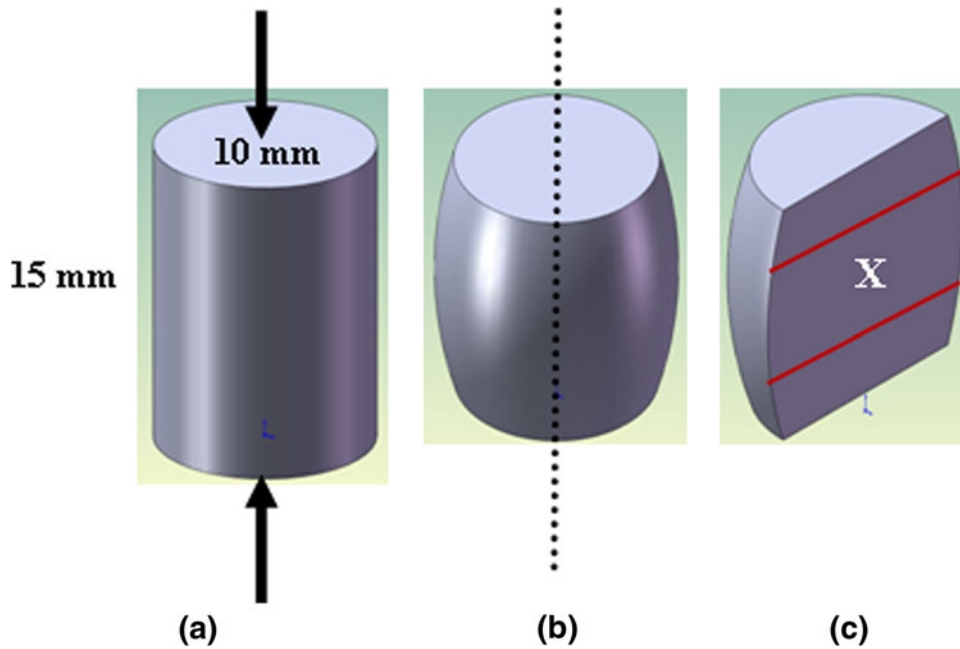| C	Mn	Si	S	P	Cr	Ni	Mo	Ti	Co	N	Fe
0.05	1.51	0.51	0.002	0.01	15.05	15.07	2.25	0.21	0.01	0.006	bal

Fig. 1—Schematic representation of the uniaxial compression specimen (*a*) before (arrow indicates the applied load direction) and (*b*) after (dotted line shows the direction along which the specimen was cut) the testing. (*c*) One half of the compressed specimen is shown (region marked "X" indicates the location where the EBSD measurements were carried out).

processed samples using a TSL-Orientation Imaging Microscopy (OIM™) system attached to an FEI Quanta 200 scanning electron microscope (FEI, Eindhoven, Netherlands) operating at 30 kV. Samples for EBSD were polished up to 0.25-μm grit diamond paste using the standard metallographic polishing procedure. Samples were further polished with colloidal silica (0.04-μm) suspension followed by electropolishing using Lectropol (Struers, Ballerup, Denmark) to ensure removal of any residual surface deformation. EBSD maps were collected from the processed samples using a step size of 0.25 to 1 μm depending on the grain size using a hexagonal grid. Standard clean-up procedure (grain dilation for single iteration) was applied before analyzing the EBSD data. In order to ensure statistical significance, the grain boundary character distribution (GBCD), average DRX grain size, and fraction of DRX in each sample were analyzed from at least two maps (area of each map ~500 × 500 μm^2) obtained from different regions. The data reported in this study are the average value obtained from these maps. The GBCD and pct DRX data are found to vary within ~3 pct. Grain orientation spread (GOS) and grain average misorientation (GAM) (evaluated from EBSD data) were analyzed to understand the microstructure development. These parameters are explained in detail elsewhere.[17,20]

III. RESULTS AND DISCUSSION

A. *Microstructural Evolution at 1173 K (900 °C)*

Typical microstructure following deformation up to a strain 0.6 at 1173 K (900 °C) at an imposed strain rate of 0.1 s^{-1} revealed deformed parent grains and twin boundaries. DRX is insignificant in these deformation conditions, and this signifies that thermal and strain energies in these conditions are not sufficient to promote DRX. At the same deformation temperature, the DRX grains were observed when the strain was increased to 0.8 at strain rates of 0.1 and 1 s^{-1} (Figures 2(a) and (b)). The DRX grains nucleate predominantly at the parent grain boundaries (shown by the arrow in Figure 2(a)). In this early stage of DRX, the pre-existing grain boundaries show serrations/bulging, due to the strain-induced boundary migration during deformation.[16] There is extensive evidence in the literature for the formation of the DRX grains (along the pre-existing grain boundaries) through the "bulging" mechanism.[12–14,18,21] It can be observed from Figure 2(a) that there are significant differences in the amplitude of these serrations/bulging in different boundaries. This could be attributed to the differences in boundary mobility, orientation of neighboring grains, and dislocation density (*i.e.*, substructure characteristics) across the boundaries.[4] In order to make a close inspection of the bulged regions of the pre-existing grain boundaries, the enclosed section in Figure 2(a) is magnified and presented in Figure 3(a). It is observed that sub-boundaries are frequently formed behind the bulged regions (shown by arrows in Figure 3(a)). It is believed that the misorientation angles of these sub-boundaries behind the bulged regions become gradually higher with increasing strain eventually resulting in the formation of DRX grains.[4] In some areas of the same specimen, the separation of the bulged region occurred through the formation of annealing twins on the bulging boundary (shown with an arrow in Figure 3(b)). However, the DRX nuclei formed through sub-boundaries behind the bulged regions appear to be mostly free of annealing twins. The DRX nuclei form on both sides of the bulged grain boundary (Figure 3(a)).
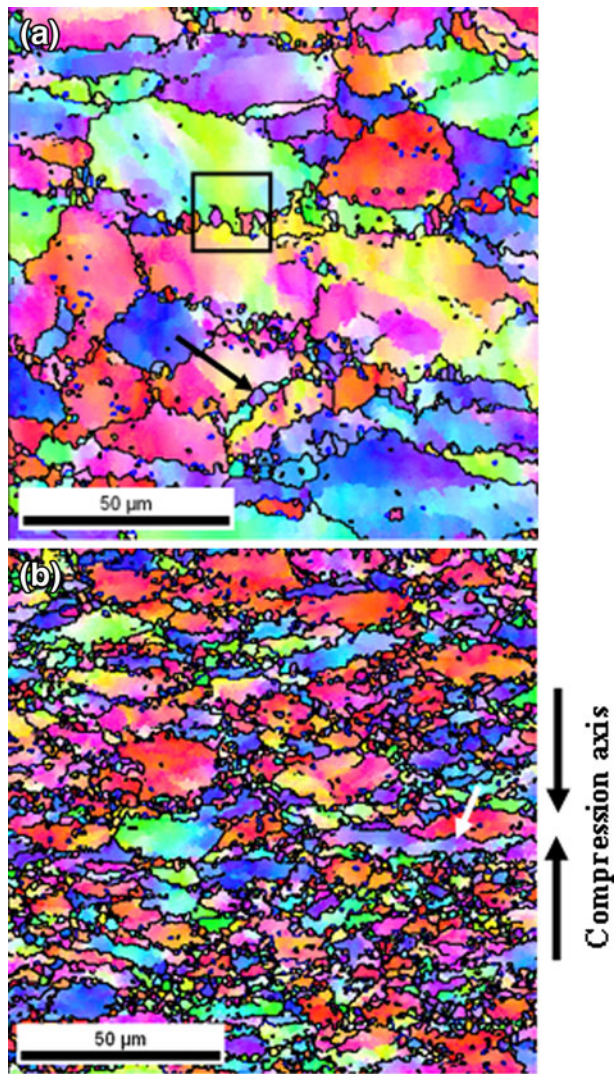
Fig. 2—IPF maps showing microstructural evolution following compression deformation at 1173 K (900 °C) to a true strain of 0.8 at (a) 0.1 and (b) 1 s^{-1} strain rate (boundary color code: Σ3—blue, other high-angle boundaries—black) (Color figure online).

A similar observation was made in a dynamically recrystallized Ni-30 pct Fe model alloy.[4] Misorientation analysis was carried out near the bulged region to evaluate the orientation gradients. The higher cumulative misorientations (*i.e.*, point-to-origin misorientation) developed across the horizontal (H) and vertical (V) lines in Figure 3(a) (Figures 3(c) and (d)) signify that a large orientation gradient developed near the bulged regions in both the perpendicular and parallel directions of the prior grain boundaries. The complexity associated with the microstructure fragmentation behind the bulged regions can potentially lead to the local formation of multiple DRX grains. Formation of several DRX nuclei could be seen near the bulged region in Figure 3(a)).

In line with the observations during the compression at 0.1 s^{-1}, the fraction of DRX grains is insignificant at 1173 K (900 °C) when the specimens are deformed up to 0.4 strain at 1 (present work), 10,[22] and 100 s^{-1} (present work). However, DRX grains are observed to

nucleate at prior grain boundaries after deformation to a strain of 0.6. At a strain of 0.8, more DRX grains nucleated at the parent grain boundaries, forming a "necklace" type structure (Figure 2(b)). However, it is also observed that in some grains (shown by arrow in Figure 2(b)), the original boundary shows no evidence of DRX. This reveals that there is an inhomogeneity in the DRX process.[23] A closer look at Figures 2(a) and (b) reveals that the fraction of DRX grains increased with an increase in strain rate from 0.1 to 1 s^{-1}.

B. Microstructural Evolution at 1273 K (1000 °C)

Grain boundary image quality (IQ) maps of samples deformed at 1273 K (1000 °C) to different strain levels at the lowest (0.1 s^{-1}) and highest (100 s^{-1}) strain rates are shown in Figures 4 and 5, respectively. It could be observed that the extent of DRX is similar at both strain rates when the imposed strain is ~0.4 (Figures 4(a) and 5(a)). Both the microstructures contain high fractions of Σ1 boundaries and deformed parent grains. The preexisting twin boundaries are found to lose their coherency due to the imposed deformation. Acceleration in DRX could be observed with increasing strain at the strain rate of 100 s^{-1}. At this strain rate, very high fractions of DRX are observed when deformed to strain of 0.6 (Figure 5(b)). However, DRX is observed to be just initiated at the same strain level at a strain rate of 0.1 s^{-1} (Figure 4(b)). The DRX grains are equiaxed, and the average size of the DRX grains (~3 μm) is similar at both strain rates. At 0.8 strain, almost a fully DRX microstructure evolved at a strain rate of 100 s^{-1} (Figure 5(c)). The microstructure reveals a very high fraction of Σ3 boundaries, which are straight and parallel in morphology, indicating that these are mainly coherent twins. The majority of the twin boundaries are found within the DRX grains, signifying that the twins were formed during the growth of the DRX grains. In contrast, a partially recrystallized microstructure with equiaxed DRX grains and elongated parent grains is observed at the same deformation level when the imposed strain rate is 0.1 s^{-1} (Figure 4(c)). From the preceding observations, it appears that DRX is enhanced at a higher strain rate with increasing strain at 1273 K (1000 °C).

C. Microstructural Evolution at 1373 K (1100 °C)

Microstructural investigation of samples deformed at 1373 K (1100 °C) reveals that a larger fraction of DRX grains (higher than those deformed at 1273 K (1000 °C)) are formed at all the strain rates. At the highest temperature and strain examined in this study, the material is still not completely recrystallized at 0.1 s^{-1} (Figure 6(a)). An appreciable amount of deformed grains exist in this specimen. The DRX fraction rapidly increases with strain rate, and the material appears to be completely recrystallized at a strain ~0.8 and at a strain rate of >1 s^{-1} (Figure 6(b)). The average size of the DRX grains (~6 μm) is almost 2 times that observed following deformation at 1273 K (1000 °C).
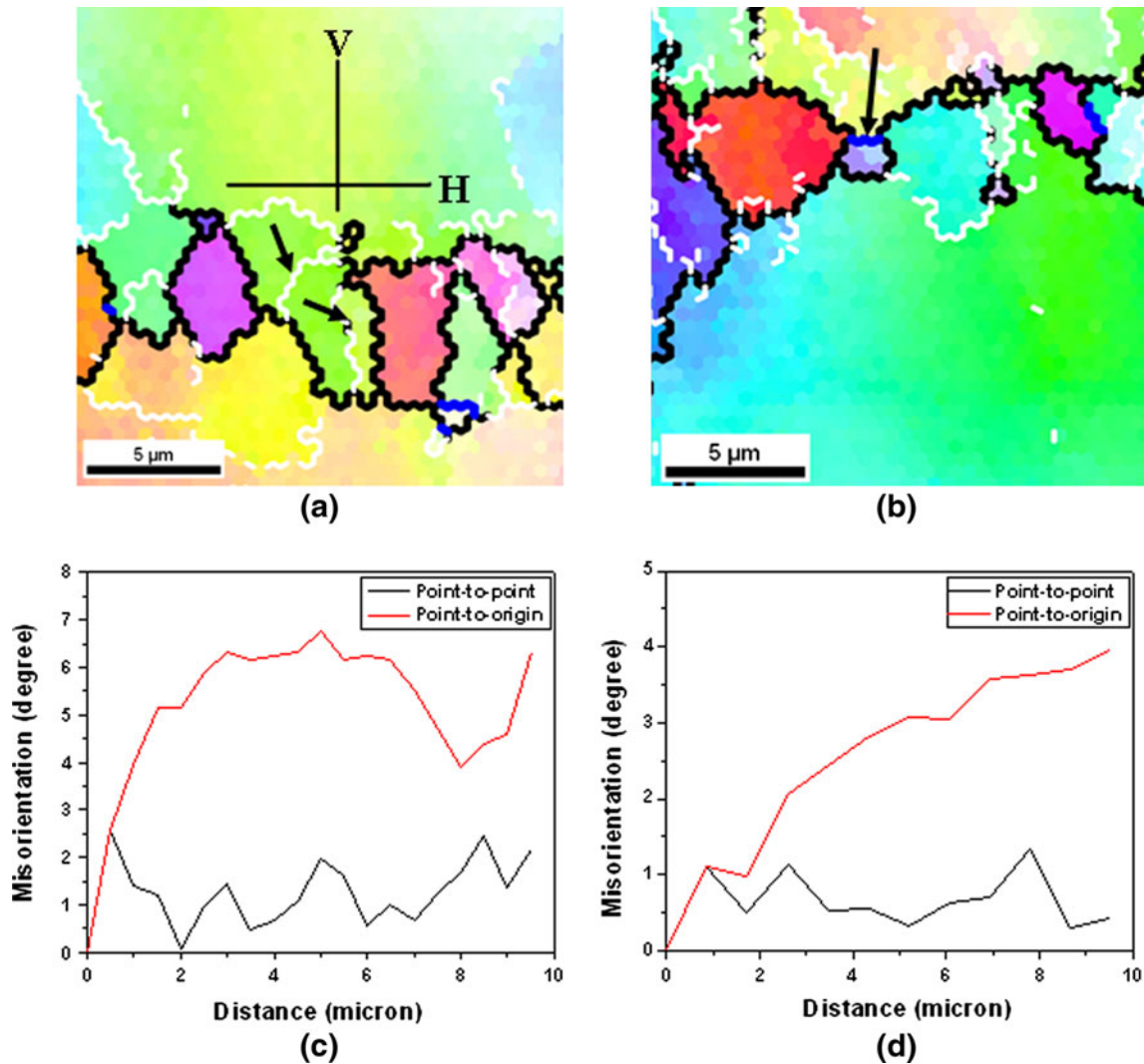
Fig. 3—(*a*) Enlarged region of Fig. 2(a) showing DRX grain formed through the bulging of pre-existing grain boundary and separation of bulge assisted through sub-boundary evolution; (*b*) separation assisted by twinning (shown by arrow); (*c*) misorientation angle changes parallel to the pre-existing grain boundary, line H in (a); and (*d*) misorientation angle changes perpendicular to the pre-existing grain boundary, line V in (a). Black, white, and blue lines in (a) and (b) represent grain boundaries with misorientation angles greater than 15 deg, between 5 and 15 deg, and Σ3 boundaries, respectively (Color figure online).

D. *Influence of Strain Rate on DRX*

To evaluate the influence of strain rate on DRX in alloy D9, the area fraction of DRX grains is partitioned out in different processing conditions employing the GOS approach. In our recent article on the influence of strain and temperature on DRX behavior of alloy D9 at a constant stain rate ($10 \ s^{-1}$), it was shown that GOS with a "cutoff" of 1 deg is a suitable criterion to partition DRX grains from the deformed matrix.[17] Employing the aforementioned criterion, the influence of strain rate on DRX at a strain of 0.6 and temperature of 1373 K is evaluated and shown in Figure 7. The top IPF maps in Figure 7 are the partitioned DRX grains, whereas the center IPF maps are the corresponding deformed grains. The inverse pole figures (IPFs) of the partitioned DRX grains at various strain rates are also shown (the IPFs at the bottom in Figure 7). It is observed that the resultant texture in the DRX grains is almost random at all the strain rates. Such a random texture is generally associated with multiple twinning.[15] Figure 7 reveals that the DRX region increases with strain rate. Quantitative estimations of the area fraction of the DRX in the specimens deformed to 0.6 and 0.8 strain at different temperatures and strain rates were made and are shown in Figure 8. It is observed that the area fraction of DRX increases with strain and temperature at all strain rates. This observation is in agreement with the established theory of DRX.[17] However, the most striking observation in Figure 8 is that the area fraction of DRX increases with strain rate at all the deformation temperatures. It may be noted here that DRX is commonly found to accelerate with the decrease in strain rate in the low strain rate domain (*i.e.*, 10^{-5} to $10^{-1} \ s^{-1}$).[5–7] However, the results of the present study clearly indicate that DRX in alloy D9 is accelerated at strain rates $>1 \ s^{-1}$. It was suggested that when the deformation time is very short due to the high strain rate, some fraction of the recrystallized grains,
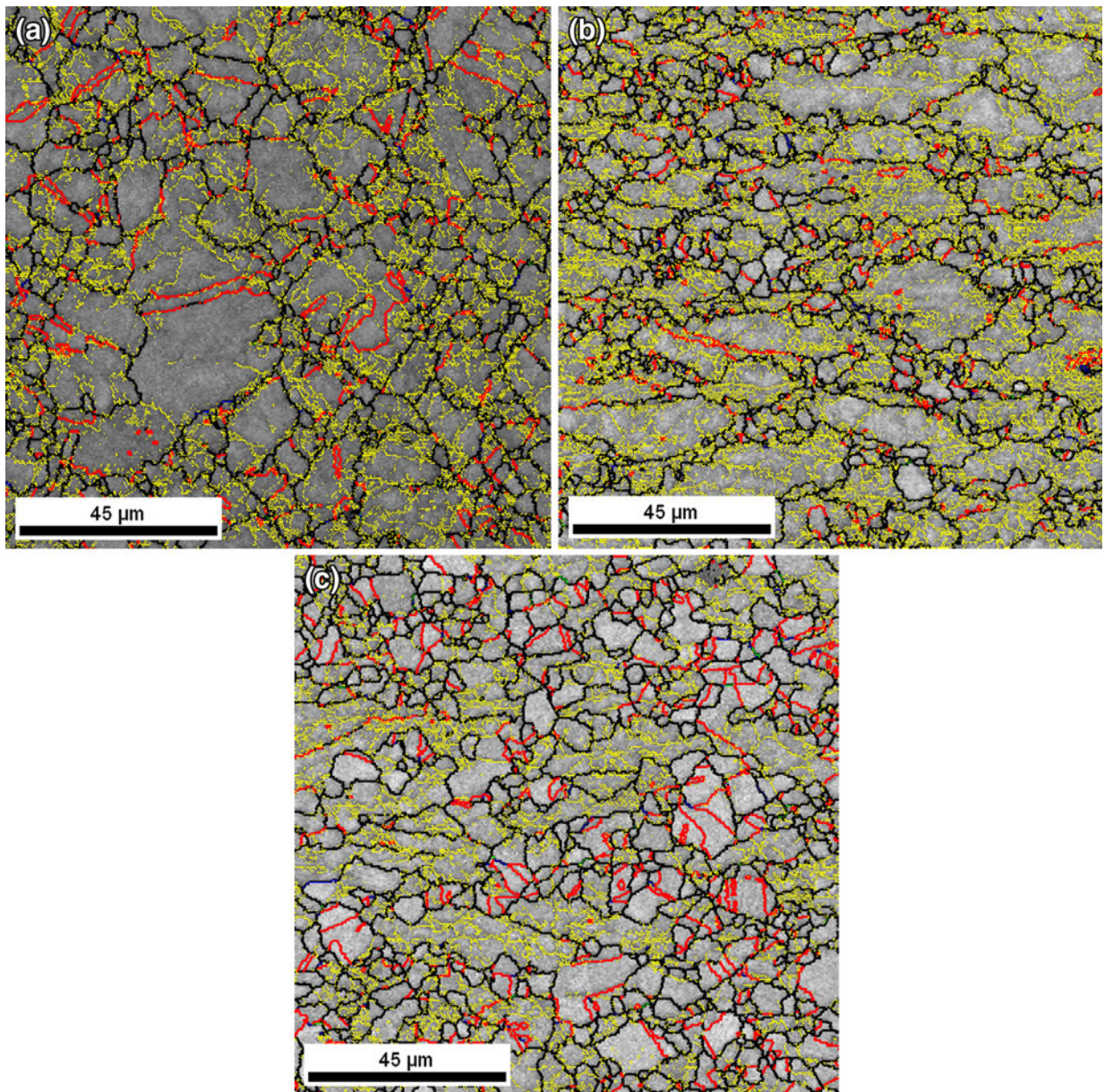
Fig. 4—IQ grain boundary maps of the specimens deformed to (*a*) 0.4, (*b*) 0.6, and (*c*) 0.8 strain at 1273 K (1000 °C) and 0.1 s^{-1} (color code: $\Sigma 3$—red, $\Sigma 9$—blue, $\Sigma 27$—green, $\Sigma 1$—yellow, and other boundaries—black) (Color figure online).

particularly at lower strains, are due to static recrystallization (SRX) owing to the delay in quenching following hot working.[14] It may be noted that in the present work, special care was taken to ensure quenching the samples within 1 to 2 seconds following hot working. Therefore, higher fractions of recrystallization at high strain rates in the present work could not be attributed to delay in quenching, *i.e.*, SRX, but to the DRX. A higher fraction of DRX was also observed following industrial scale thermomechanical processing at a high strain rate (during hammer forging operation with a mean strain rate ~100 s^{-1}) in alloy D9.[24] DRX was found to be nearly completed at 1373 K (1100 °C) and 0.5 strain during the hammer forging operation. However, the DRX was far from complete in similar deformation conditions during the hydraulic press

forging operation (mean strain rate is ~0.2 s^{-1}).[24] Acceleration of DRX was also observed at high strain rates (10 to 50 s^{-1}) in duplex stainless steel in the temperature range 1348 to 1423 K (1075 to 1150 °C).[25] The twin density and the fraction of DRX were also reported to increase with the strain rate in the ZK60 alloy[26] and Allvac 718PLUS.*[19]

---

*718 PLUS is a trademark of Allegheny Technologies International, Pittsburgh, PA.

The acceleration of DRX at higher strain rates in alloy D9 could be attributed to the increased rate of dislocation accumulation as well as the adiabatic temperature rise. Dislocation density increases with increasing strain rate
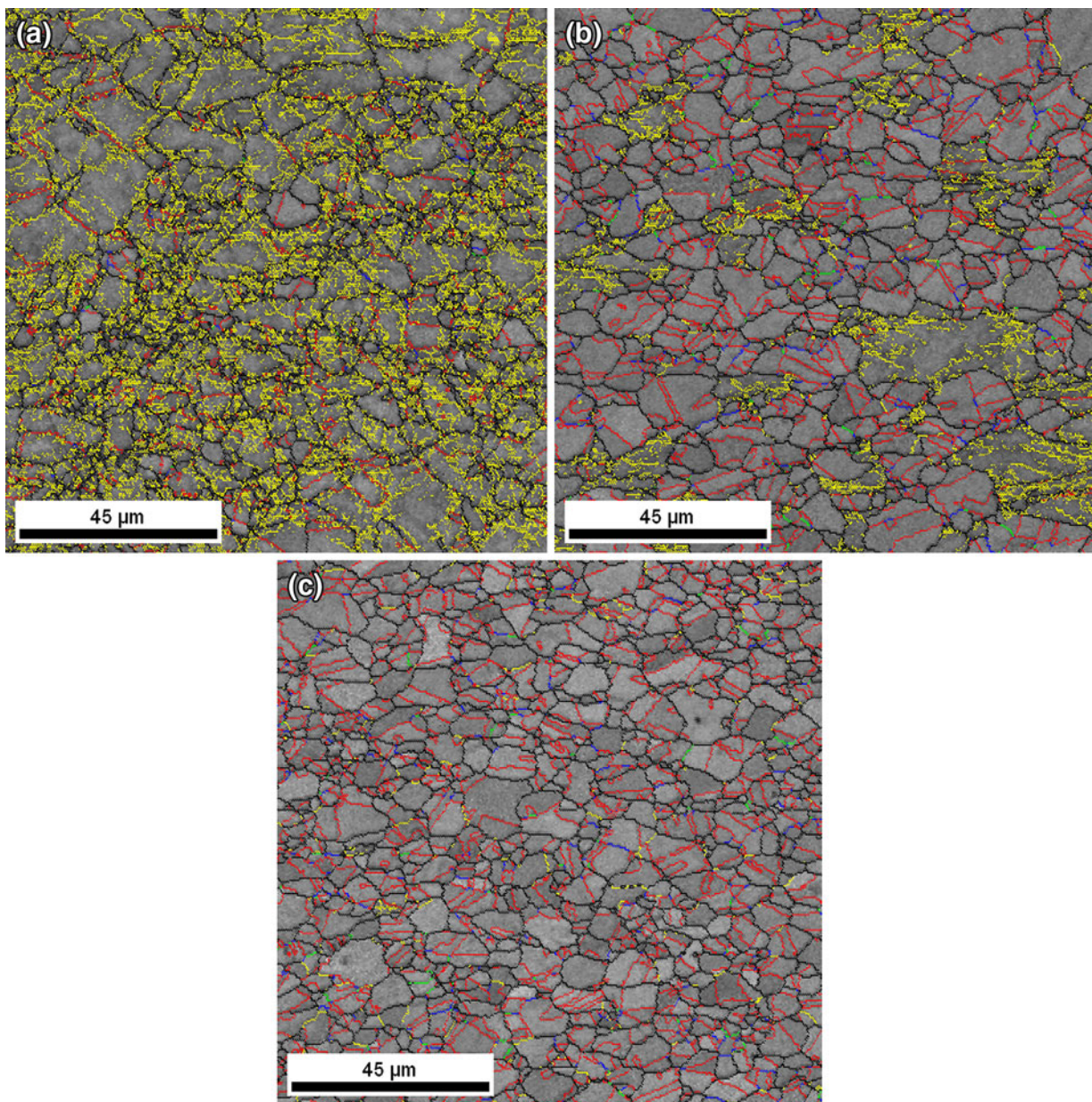
Fig. 5—IQ grain boundary maps of the specimens deformed to (*a*) 0.4, (*b*) 0.6, and (*c*) 0.8 at 1273 K (1000 °C) and 100 s^{-1} (color code: same as in Fig. 4) (Color figure online).

due to a strong dislocation–dislocation interaction and weak recovery.[27] Therefore, it is expected that a higher strain rate would lead to an increase in the dislocation density (*i.e.*, stored energy) in the material. This, in turn, would significantly reduce the temperature required for recrystallization. There are reports in the literature showing that high stored energy significantly reduces the recrystallization temperature.[26,28] During high strain rate deformation, a large amount of plastic work and frictional work is converted to heat, while less heat is transferred to surroundings due to the relatively short contact time. This leads to an adiabatic temperature rise within the specimen. The adiabatic temperature rise is beneficial for DRX nucleation and the grain boundary

migration that eventually accelerates the DRX process. DRX was found to accelerate by adiabatic temperature rise during high strain rate deformation in Cu and Mg alloys.[8,26,28] In contrast to this, the adiabatic temperature rise at low strain rates would be insignificant as heat can transfer to surroundings due to longer contact time. It is also important to note that there would be fewer dislocation-dislocation interactions in the low strain rate domain. Thereby, it is apparent that an increase in the dislocation density (*i.e.*, stored energy) due to an increase in strain rate in this domain would be insignificant. The acceleration of DRX with the decrease in strain rate in the low strain rate domain[5–7] is mainly due to longer deformation times available for nucleation and growth of DRX grains.
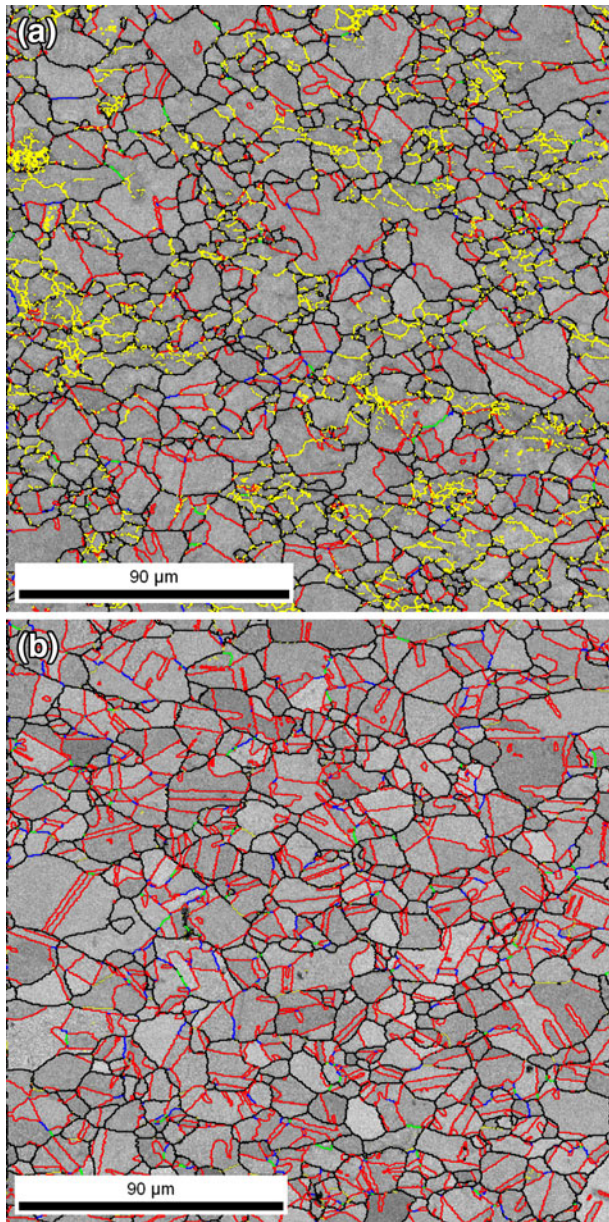
Fig. 6—IQ grain boundary maps of the specimens deformed at 1373 K (1100 °C) to a true strain of 0.8 at (*a*) 0.1 and (*b*) 100 s^{-1} strain rate.

E. *Evolution of $\Sigma 1$, $\Sigma 3$, and $\Sigma 9$ Boundaries*

A quantitative estimation of $\Sigma 1$, $\Sigma 3$, and $\Sigma 9$ boundaries at various strains and strain rates at a particular temperature (*i.e.*, 1273 K (1000 °C)) is shown in Figure 9. It is observed that the strain rate has little influence on the evolution of these boundaries at a strain of 0.4. However, significant influence of strain rate is observed at strains above 0.4. A moderate decrease in $\Sigma 1$ boundary fraction with strain is observed at the lowest strain rate (*i.e.*, 0.1 s^{-1}) (Figure 9(a)). However, the decrease in $\Sigma 1$ boundary fraction with strain is pronounced at higher strain rates (*i.e.*, 10 and 100 s^{-1}). This signifies that low-angle boundaries are predominantly eliminated by the migrating high-angle grain boundaries during deformation at higher strain rates.

The acceleration of DRX at high strain rate has already been emphasized in Section III–D. The increase in $\Sigma 3$ boundary fraction with strain is only marginal at 0.1 s^{-1} (Figure 9(b)). However, a significant increase in $\Sigma 3$ boundary fraction with strain is observed at 10 and 100 s^{-1}. This indicates that the formation of twin boundaries is accelerated at higher strain rates. This is attributed to the increased rate of grain boundary migration due to adiabatic temperature rise during high strain rate deformation.

The trend of $\Sigma 9$ boundary evolution with strain and strain rate (Figure 9(c)) is quite similar to that of $\Sigma 3$ boundaries (Figure 9(b)). The fraction of $\Sigma 9$ boundaries remains constant at all strain levels when the hot deformation was carried out at 0.1 s^{-1}. Though a noticeable increase in $\Sigma 9$ boundary fraction is observed at higher strain rates (*i.e.*, 10 and 100 s^{-1}), the absolute increase is only marginal (Figure 9(c)). For example, it has increased to ~3 pct at 0.8 true strain as compared to ~1 pct at 0.4 true strain when hot deformation was carried out at 100 s^{-1} and 1273 K (1000 °C). This signifies that generation of secondary annealing twins is insignificant even at 100 s^{-1} when DRX is predominant.

F. *Origin of $\Sigma 3$ Boundaries*

It was observed in Figures 4 through 6 that the majority of the DRX grains are twinned. In order to understand the evolution of twins during DRX, fractions of $\Sigma 3$ boundaries at different DRX levels (at all strain rates) were calculated (Figure 10(a)). It can be seen that the $\Sigma 3$ boundary fraction increased linearly with the area fraction of DRX. It may be noted here that according to the Brandon's criterion,[29] if the boundary misorientation deviates by less than 8.7 deg from the reference misorientation of 60 deg about the $\langle 111 \rangle$ axis, it is categorized as $\Sigma 3$ boundary. However, this classification includes coherent twins, incoherent twins, as well as other $\Sigma 3$ boundaries whose misorientations fall within the Brandon's criterion but may not have been formed by the twinning mechanism.[30] Though all these boundaries are classified as $\Sigma 3$ boundaries, they have different interfacial planes and, hence, different properties. Even though the two-dimensional EBSD cannot identify the type of $\Sigma 3$ boundaries, postprocessing of the misorientation data can be used to estimate the type of $\Sigma 3$ boundaries with good statistical accuracy and reliability.[30,31] For example, coherent twins usually have misorientation angles less than 1.7 deg away from ideal $\langle 111 \rangle$ 60 deg misorientation (*i.e.*, ~20 pct of the upper deviation limit of 8.7 deg per Brandon criterion).[30] Likewise, incoherent twins generally have higher deviation from the reference misorientation, while the other $\Sigma 3$ boundaries (*i.e.*, excluding coherent and incoherent twin boundaries) have much larger deviations. Applying the aforementioned criterion, fractions of coherent twin boundaries were calculated in all the different specimens and correlated to the area fraction of DRX (Figure 10(a)). It is observed that, similar to $\Sigma 3$ boundaries, a linear relationship exists between the area fraction of DRX and the fraction of coherent twin boundaries. In
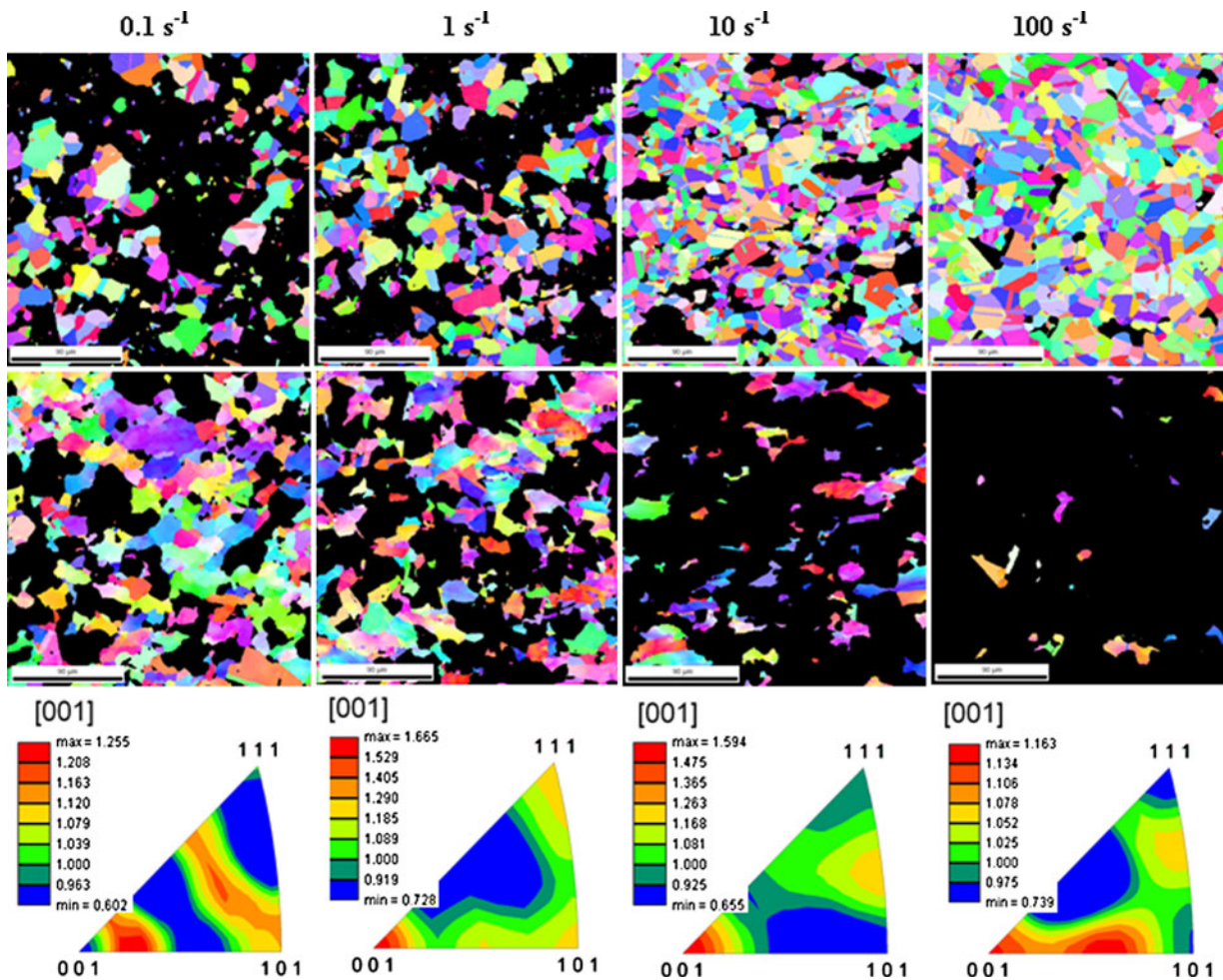
Fig. 7—IPF maps of the partitioned DRX grains (top), deformed grains (center), and the IPFs of the partitioned DRX grains (bottom) at different strain rates at 1373 K (1100 °C) and 0.6 strain.
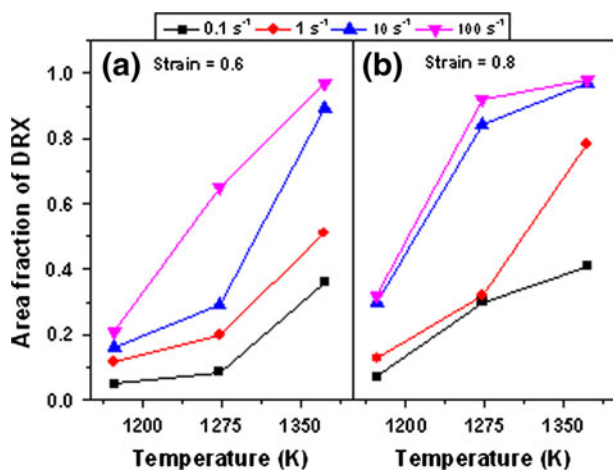

Fig. 8—Area fraction of DRX in the specimens deformed to a strain of (a) 0.6 and (b) 0.8 at different temperatures and strain rates.

addition, a closer look at Figure 10(a) reveals that the majority of the Σ3 boundaries are coherent twin boundaries. The correlation between the area fraction of DRX and Σ9 boundaries also shows a linear relationship (Figure 10(b)). However, unlike Σ3 (and coherent twin boundaries), the absolute increase in Σ9 boundaries during DRX is only marginal. For example, Σ9 boundaries have increased to ~3 pct in fully DRX structure as compared to ~1 pct in a partially recrystallized (area fraction of DRX is ~20 pct) microstructure. It may be noted here that interaction between two Σ3 boundaries forms a Σ9 boundary according to the relationship[32]

$$\Sigma 3 + \Sigma 3 = \Sigma 9 \qquad [1]$$

The marginal increase in Σ9 boundaries with DRX fraction (Figure 10(b)) indicates that interaction between Σ3 boundaries happened infrequently during DRX.

The origin of coherent twin boundaries during DRX now needs to be investigated. It could be argued that the source of these coherent twin boundaries is the preexisting twin boundaries in the SA specimen. This view may stem from the fact that the SA specimen contains a large proportion (~47 pct) of Σ3 boundaries. However, it was observed that the average deviation of Σ3 boundaries from ideal misorientation (⟨111⟩ by 60 deg)
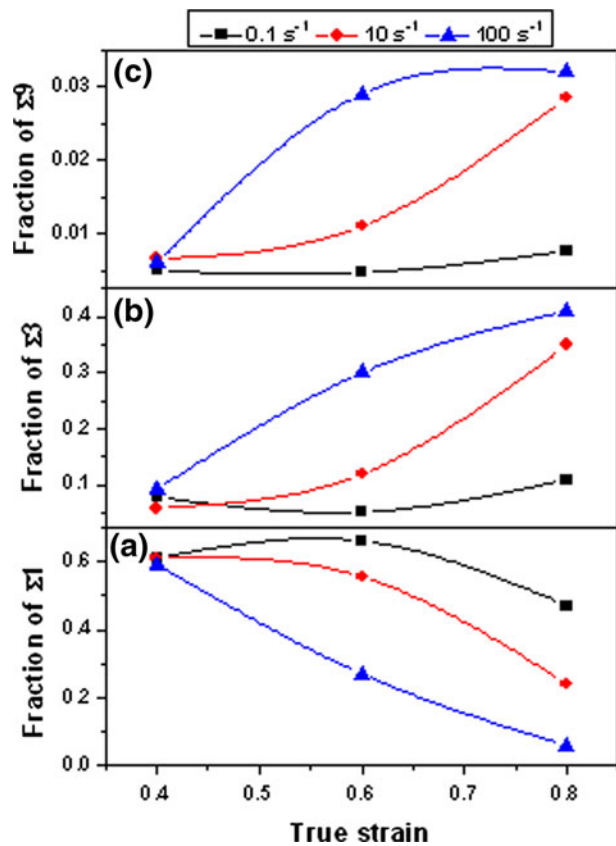
Fig. 9—Fraction of (a) Σ1, (b) Σ3, and (c) Σ9 boundaries following hot compression to different strains and strain rates at 1273 K (1000 °C).

Fig. 10—Variation of fraction of (a) Σ3 and coherent twin boundaries and (b) Σ9 boundaries with area fraction of DRX.

Fig. 11—Deviation of Σ3 boundaries from ideal orientation at different DRX level.

decreased with the increase in deformation at all temperatures after DRX was initiated.[17] The decrease in average deviation with increase in imposed deformation signifies that the majority of these Σ3 boundaries were newly generated. Otherwise, an increase in the imposed deformation level would have increased the average deviation of these Σ3 boundaries. The average deviation of these Σ3 boundaries at various DRX levels at all strain rates was also calculated and is shown in Figure 11. It is observed that the average deviation decreases almost exponentially with the area fraction of DRX at all imposed strain rates. This indicates that the Σ3 boundaries are closer to the ideal orientation at higher DRX fractions. This further signifies that most of the Σ3 boundaries are newly formed during DRX. The GAM of the microstructures evolved at all imposed strain rates is correlated to the fraction of Σ3 boundaries and is presented in Figure 12. It is clear that there is an inverse correlation between the fraction of Σ3 boundaries and the GAM. The lower GAM (GAM being an index of point-to-point misorientation or local strain) associated with the higher Σ3 fraction indicates that the Σ3 twins are relatively free of deformation. This further signifies that the observed twins are freshly nucleated.[33]

It is generally believed that the formation of Σ3 twins during DRX is due to grain boundary migration,[18,34,35] as in the case of annealing twins,[36] and not due to slip activity within grains.[35] It may be noted that new Σ3
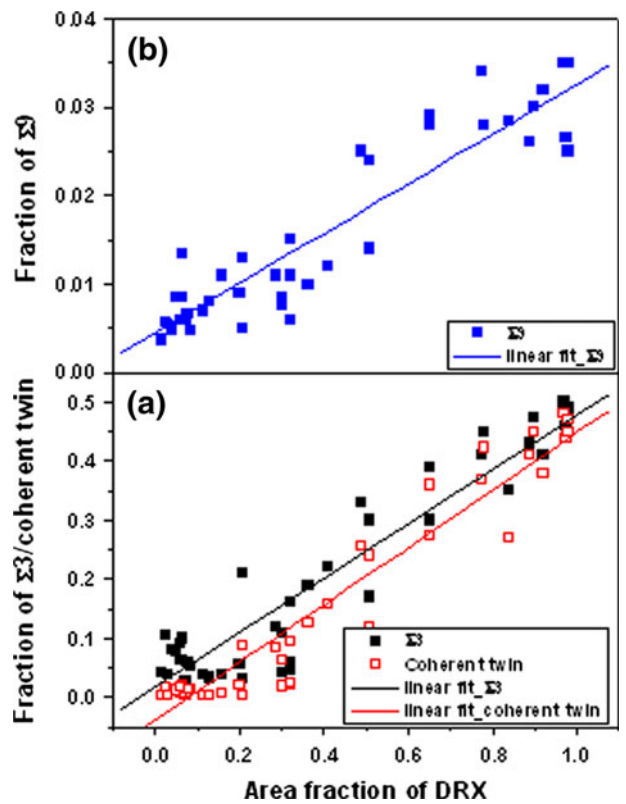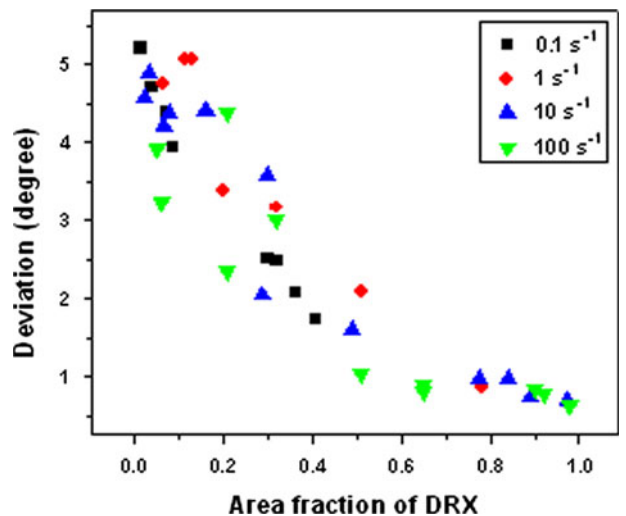
boundaries may form due to the interaction of pre-existing Σ3 boundaries (per Eq. [1]) during grain boundary migration[37] or by "growth accidents" during recrystallization.[38] Interaction of pre-existing Σ3 boundaries may form first a Σ9 boundary, as discussed earlier. Similarly, interaction between a Σ3 and Σ9 may form a Σ3 boundary.[39] If these interactions occur

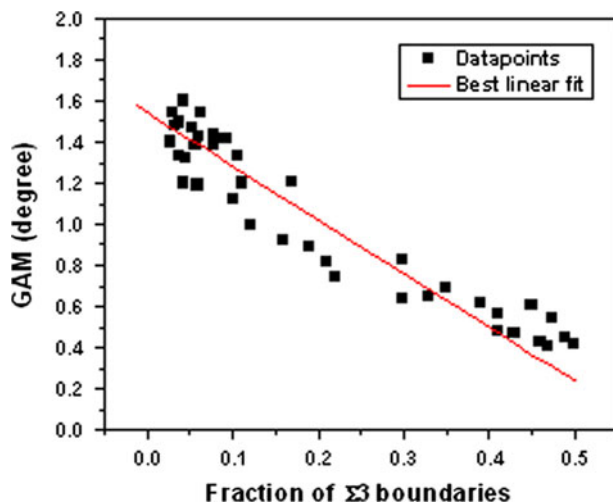Fig. 12—GAM as a function of the fraction of Σ3 boundaries obtained in different processing conditions.

Fig. 13—IPF map of the specimen deformed at 1173 K (900 °C) and 10 s^{-1} to true strain of 0.8, showing how twins help to separate the bulged portions from the parent grains. Black, white, yellow, and blue lines represent boundaries with misorientation angles greater than 15 deg, between 5 and 15 deg, less than 5 deg, and Σ3 boundaries, respectively.

predominantly, then the increase in Σ3 boundary would invariably be associated with a significant increase in Σ9 boundaries.[37] However, it was observed (Figures 9(c) and 10(b)) that an increase in Σ9 boundaries during DRX is not significant. Therefore, it can be inferred that the interaction of pre-existing Σ3 boundaries that may regenerate Σ3 boundaries did not occur frequently during DRX. The increase in Σ3 boundaries, therefore, can be attributed to the formation of annealing twins during DRX. During the growth of nucleated DRX grains, growth accidents may occur at the moving grain boundary and generate twin boundaries. This is consistent with our observations that the majority of the annealing twins were formed within the DRX grains (Figures 4 through 6), suggesting that these were mostly formed during the growth of DRX grains. A similar observation was made by Miura *et al*.[7] during DRX in Cu alloy bicrystals. It was suggested that the density of these annealing twins formed by growth accidents largely depends on the driving force for grain boundary migration.[40] This is in line with our observations that higher fractions of Σ3 boundaries were formed at higher strain rates (*i.e.*, 10 and 100 s^{-1}) (Figure 9(b)). The formation of annealing twins is further accelerated during the DRX process, since the deformation is continuously applied; this may produce more {111} steps on the boundaries, which would, in turn, increase the probability of twin formation.[36]

Although annealing twins were mostly observed to form during the growth stage, few of them are found to emanate during the nucleation stage itself at both the high strain rates (arrowed boundaries in Figure 13) and low strain rates (arrowed boundary in Figure 3(b)). The mechanism for twin formation inside the subgrain structure during the nucleation stage of DRX is not clear. In single crystals, the generation of twins was suggested to be triggered by dislocation interactions in the subgrain boundary, *e.g.*, by a pole mechanism or dissociation of appropriate pre-existing assemblies of dislocations.[41] Twin lamella were found to emanate from sub-boundaries while being investigated via transmission electron microscopy in Cu
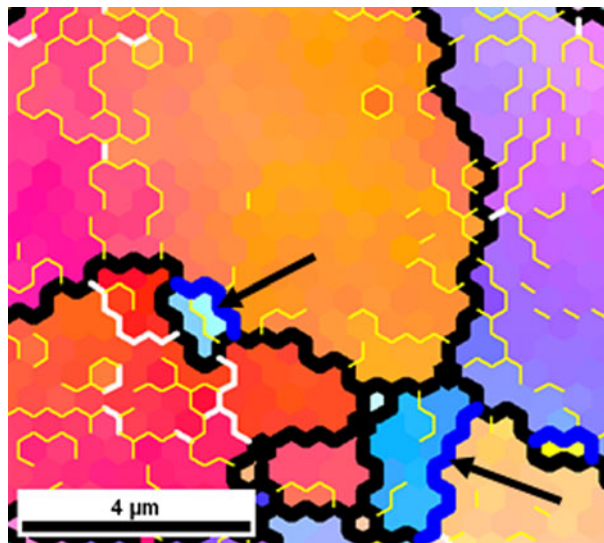
single-crystal[42] and polycrystalline alloy 800H,[18] which gives evidence for the twin generation by the motion of partial dislocations.

G. *Role of Annealing Twin on DRX*

The generations of twin boundaries during recrystallization (both static and dynamic) were reported in a wide variety of low SFE materials.[5,18,19,33,42,43] We believe that these annealing twins play a significant role in nucleation and the growth process during DRX. It should be noted here that the role of low SFE on the occurrence of DRX was traditionally associated with an increase in stored energy caused by the inhibition of climb and cross-slip.[1] However, it was suggested that the low SFE may play an additional role in promoting DRX.[42] This supplementary role is linked to the likelihood of forming annealing twins during hot deformation of low SFE materials. While materials with high SFE are known to exhibit high twin boundary energies, and hence are not likely to form annealing twins, low SFE promotes the formation of annealing twins due to the lowering of twin boundary interfacial energy.

The role of annealing twins on DRX now needs to be discussed. Twinning due to growth accidents will change the growth rate and may add to the nucleation rate, thereby influencing the kinetics of DRX.[18] Annealing twins would help growth resume when stagnation of grain growth occurred during DRX. This is due to the fact that the boundary/interface between the recrystallized grains and the deformed matrix after growth stagnation was often found to be a region of low misorientation or low dislocation density.[43] Twinning at the interface would essentially change the misorientation and, thereby, provide additional boundary energy required for migration and growth. Such twinning in the

interface not only allows the DRX volume to grow perpendicular to the interface, but also in the parallel direction.[18] It was shown by a three-dimensional EBSD analysis in a dynamically recrystallized Cu-Sn bronze that DRX is propagated by successive twinning from the few nucleated grains, along the prior grain boundaries, resulting in several hundred twins related DRX grains.[44] Although the majority of the twin boundaries form during the growth of the DRX grains, there are indications that twinning at the interface may accelerate the bulging process[5] and help in separation of the bulged region from the parent grain.[45,46] The appearance of twin boundaries during the bulging process was also observed in the present study. It was observed that twin boundaries assist in separating the bulged portion from the pre-existing high-angle boundaries at both low strain rate (arrow in Figure 3(b)) and high strain rate (arrowed regions in Figure 13) deformation conditions and, thereby, play an important role during nucleation and subsequent expansion of the DRX process in alloy D9.

IV. CONCLUSIONS

Microstructural evolution and DRX behavior in alloy D9 during moderate to high strain rate (0.1 to 100 s^{-1}) hot deformation (1173 to 1373 K) (900 to 1100 °C range) was studied by performing uniaxial compression testing in a thermomechanical simulator. The origin and role of twin boundaries on DRX was investigated. From this study, the following conclusions are derived.

1. Nucleation of new DRX grains occurred by the serrations/bulging of the parent grain boundary, and significant differences in the amplitude of these serrations/bulging in different boundaries were observed. This was attributed to the differences in boundary mobility, orientation of neighboring grains, and dislocation density (i.e., substructure characteristics) across the boundaries.
2. Misorientation analysis near the bulged region of the prior grain boundaries revealed that large orientation gradients developed near the bulged regions, in both the perpendicular and parallel directions of the prior grain boundaries, leading to the nucleation of multiple DRX grains. The complexity associated with the microstructure fragmentation behind the bulged regions could potentially lead to the formation of multiple DRX grains.
3. The extent of DRX was found to increase with increasing strain rate in the range of hot working parameters employed in the present study. The acceleration of DRX at higher strain rates was attributed to an increased rate of dislocation accumulation due to a strong dislocation–dislocation interaction (and weak recovery) as well as adiabatic temperature rise.
4. The DRX grains were observed to be associated with $\Sigma 3$ boundaries. Based on the misorientation analysis, it was observed that the majority of the $\Sigma 3$ boundaries are coherent twin boundaries. The deviation of these boundaries from ideal misorientation

($\langle 111 \rangle$ by 60 deg) decreased with the increase in strain and the area fraction of DRX at all strain rates, signifying that most of the $\Sigma 3$ twin boundaries were newly formed during DRX. This was further confirmed by GAM measurements.
5. Quantitative estimation of $\Sigma 3$ and $\Sigma 9$ boundaries revealed a marginal increase in $\Sigma 9$ boundaries with DRX fraction, suggesting that interaction of pre-existing $\Sigma 3$ boundaries, which could have regenerated $\Sigma 3$ twin boundaries, did not occur frequently during DRX. The majority of the $\Sigma 3$ twin boundaries were present within the DRX grains, signifying that these were annealing twins formed mainly by growth accidents during the growth stage of the DRX grains.
6. Formation of twin boundaries is accelerated at higher strain rates (10 and 100 s^{-1}) due to the increased rate of grain boundary migration, which is a consequence of adiabatic temperature rise. Although the majority of these annealing twins were formed during the growth of DRX grains, a few of these twins were also found to emanate during the nucleation stage. These annealing twins played an important role during nucleation and subsequent expansion of the DRX region in alloy D9.

REFERENCES

1. R.W. Cahn and P. Haasen: *Physical Metallurgy*, Cambridge University Press, New York, NY, 1996, vol. III.
2. I.P. Pinheiro, R. Barbosa, and P.R. Cetlin: *Mater. Sci. Eng. A*, 2007, vol. 457, pp. 90–93.
3. P. Poelt, C. Sommitsch, S. Mitsche, and M. Walter: *Mater. Sci. Eng. A*, 2006, vol. 420, pp. 306–14.
4. H. Beladi, P. Cizek, and P.D. Hodgson: *Metall. Mater. Trans. A*, 2009, vol. 40A, pp. 1175–89.
5. Y. Wang, W.Z. Shao, L. Zhen, L. Yang, and X.M. Zhang: *Mater. Sci. Eng. A*, 2008, vol. 497, pp. 479–86.
6. A.G. Beer and M.R. Barnett: *Metall. Mater. Trans. A*, 2007, vol. 38A, pp. 1856–67.
7. H. Miura, M. Ozama, R. Mogawa, and T. Sakai: *Scripta Mater.*, 2003, vol. 48, pp. 1501–05.
8. U. Andrade, M.A. Meyers, K.S. Vecchio, and A.H. Chokshi: *Acta Metall. Mater.*, 1994, vol. 42, pp. 3183–95.
9. R.D. Doherty, D.A. Hughes, F.J. Humphreys, J.J. Jonas, D. Juul Jensen, M.E. Kassner, W.E. King, T.R. McNelley, H.J. McQueen, and A.D. Rollett: *Mater. Sci. Eng. A*, 1997, vol. 238, pp. 219–74.
10. T. Sakai and J.J. Jonas: *Acta Metall.*, 1984, vol. 32, pp. 189–209.
11. H.J. McQueen: *Mater. Sci. Eng. A*, 2004, vols. 387–389, pp. 203–08.
12. A. Belyakov, H. Miura, and T. Sakai: *Mater. Sci. Eng. A*, 1998, vol. 255, pp. 139–47.
13. A. Dehghan-Manshadi, H. Beladi, M.R. Barnett, and P.D. Hodgson: *Mater. Sci. Forum*, 2004, vols. 467–470, pp. 1163–68.
14. A. Dehghan-Manshadi, M.R. Barnett, and P.D. Hodgson: *Metall. Mater. Trans. A*, 2008, vol. 39A, pp. 1359–70.
15. D. Ponge and G. Gottstein: *Acta Mater.*, 1998, vol. 46, pp. 69–80.
16. F.J. Humphreys and M. Hatherly: *Recrystallization and Related Annealing Phenomena*, Pergamon-Elsevier, Oxford, United Kingdom, 2004.
17. S. Mandal, A.K. Bhaduri, and V. Subramanya Sarma: *Metall. Mater. Trans A*, 2011, vol. 42A, pp. 1062–72.
18. E. Brünger, X. Wang, and G. Gottstein: *Scripta Mater.*, 1998, vol. 38, pp. 1843–49.
19. S. Mitsche, C. Sommitsch, D. Huber, M. Stockinger, and P. Poelt: *Mater. Sci. Eng. A*, 2011, vol. 528, pp. 3754–60.

20. S. Mandal, S.K. Mishra, A. Kumar, I. Samajdar, P.V. Sivaprasad, T. Jayakumar, and B. Raj: *Philos. Mag.*, 2008, vol. 88, pp. 883–97.
21. W. Roberts and B. Ahlblom: *Acta Metall.*, 1978, vol. 26, pp. 801–13.
22. S. Mandal, P.V. Sivaprasad, and V. Subramanya Sarma: *Mater. Manufact. Process.*, 2010, vol. 25, pp. 54–59.
23. M. Jafari and A. Najafizadeh: *Mater. Sci. Eng. A*, 2009, vol. 501, pp. 16–25.
24. S. Mandal, P.V. Sivaprasad, and R.K. Dube: *J. Mater. Sci.*, 2007, vol. 42, pp. 2724–34.
25. Y. Han, D. Zou, Z. Chen, G. Fan, and W. Zhang: *Mater. Charact.*, 2011, vol. 62, pp. 198–203.
26. S.Q. Zhu, H.G. Yan, J.H. Chen, Y.Z. Wu, J.Z. Liu, and J. Tian: *Scripta Mater.*, 2010, vol. 63, pp. 985–88.
27. T. Sakai and M. Ohashi: *Mater. Sci. Technol.*, 1990, vol. 6, pp. 1251–57.
28. H.Q. Sun, Y.N. Shi, M.X. Zhang, and K. Lu: *Acta Mater.*, 2007, vol. 55, pp. 975–82.
29. D.G. Brandon: *Acta Metall.*, 1966, vol. 14, pp. 1479–84.
30. H. Davies and V. Randle: *Mater. Sci. Technol.*, 2000, vol. 16, pp. 1399–1402.
31. V. Randle: *J. Mater. Sci.*, 2005, vol. 40, pp. 853–59.
32. L.C. Lim and R. Raj: *Acta Metall.*, 1984, vol. 32, pp. 1177–81.
33. R. Kapoor, B. Paul, S. Raveendra, I. Samajdar, and J.K. Chakravartty: *Metall. Mater. Trans. A*, 2009, vol. 40A, pp. 818–27.
34. X. Wang, E. Brunger, and G. Gottstein: *Scripta Mater.*, 2002, vol. 46, pp. 875–80.
35. H. Miura, T. Sakai, R. Mogawa, and G. Gottstein: *Scripta Mater.*, 2004, vol. 51, pp. 671–75.
36. S. Mahajan, C.S. Pande, M.A. Imam, and B.B. Rath: *Acta Mater.*, 1997, vol. 45, pp. 2633–38.
37. S. Mandal, P.V. Sivaprasad, B. Raj, and V. Subramanya Sarma: *Metall. Mater. Trans. A*, 2008, vol. 39A, pp. 3298–3307.
38. H. Gleiter: *Acta Metall.*, 1969, vol. 17, pp. 1421–28.
39. G. Owen and V. Randle: *Scripta Mater.*, 2006, vol. 55, pp. 959–62.
40. C.S. Pande, M.A. Imam, and B.B. Rath: *Metall. Trans. A*, 1990, vol. 21A, pp. 2891–96.
41. P. Karduck, G. Gottstein, and H. Mecking: *Acta Metall.*, 1983, vol. 31, pp. 1525–36.
42. V.M. Sample, G.L. Fitzsimonss, and A.J. DeArdo: *Acta Metall.*, 1987, vol. 35, pp. 367–79.
43. D.P. Field, L.T. Bradford, M.M. Nowell, and T.M. Lillo: *Acta Mater.*, 2007, vol. 55, pp. 4233–41.
44. A. Gholinia, I. Brough, J. Humphreys, D. McDonald, and P. Bate: *Mater. Sci. Technol.*, 2010, vol. 26, pp. 685–90.
45. A.M. Wusatowska-Sarnek, H. Miura, and T. Sakai: *Mater. Sci. Eng. A*, 2002, vol. 323, pp. 177–86.
46. Y. Wang, W.Z. Shao, L. Zhen, and X.M. Zhang: *Mater. Sci. Eng. A*, 2008, vol. 486, pp. 321–32.